

Superconductivity-induced Resonance Raman Scattering
in Multi-layer High- T_c Superconductors

Mikhail Limonov,* Sergey Lee, and Setsuko Tajima,

¹*SRL-ISTEC, 10-13, Shinonome 1-Chome, Koto-ku, Tokyo 135-0062, Japan*

Akio Yamanaka

²*Chitose Institute of Science and Technology, Chitose, Hokkaido 066-8655, Japan*

Resonant Raman scattering below T_c has been discovered in several Bi-, Hg-, Tl-based high- T_c superconductors with three or four CuO_2 -layers. For $\text{Bi}_2\text{Si}_2\text{Ca}_2\text{Cu}_3\text{O}_{10+\delta}$, we found an unexpected crossover of the pair-breaking peak in the A_{1g} -spectrum from a broad bump at $\hbar\omega = 6k_B T_c$ for $E_{\text{exc}} = 2.54\text{eV}$ to a sharp peak at $\hbar\omega = 8k_B T_c$ for $E_{\text{exc}} = 2.18\text{eV}$, together with a strong enhancement of the Ca-phonons. Under resonant conditions, the relative positions of the pair breaking peaks in A_{1g} , B_{1g} , and B_{2g} channels are $2\Delta(A_{1g}) = 2\Delta(B_{1g}) > 2\Delta(B_{2g})$. This relation implies that the A_{1g} Raman channel is free from the Coulomb screening effect, just as predicted theoretically for a d-wave multi-layer superconductor but have never been observed experimentally thus far. The observed resonance effect is the evidence that the electronic state in the inner CuO_2 -planes is different from that of the outer CuO_2 -planes.

PACS numbers: 74.25.Gz, 74.72.Bk, 78.20.-e, 78.30.-j

Correspondent author : S.Tajima (tajima@istec.or.jp)

I. INTRODUCTION

A layered structure together with a strong electron correlation in high- T_c superconducting cuprates (HTSC) produces a large anisotropy in their electronic state, resulting in an incoherent charge transport in the out-of-plane direction [1] which cannot be expected from conventional band theory. In the superconducting state, owing to a short coherence length, the system can be regarded as a stack of Josephson-coupled-layers where each CuO_2 -plane is an independent superconducting layer [2]. In the case of compounds with multiple CuO_2 -layers in a formula unit, the multi-sheet effect manifests itself in the peculiar charge response such as the double Josephson plasma accompanied with an additional absorption peak [3]. Another report of multi-sheet effect is the splitting of the Fermi surface observed in the angle-resolved photoemission spectroscopy on the heavily overdoped $(\text{Bi,Pb})_2\text{Sr}_2\text{CaCu}_2\text{O}_8$ [4]. In the nuclear magnetic resonance experiment, it is indicated that the doping level of the inner CuO_2 -planes is lower than that of the outer planes [5]. So far, most of the theories for HTSC deal with the electronic state only within the CuO_2 -planes, ignoring the structure in the out-of-plane direction. However, it is empirically known that layer-stacking strongly affects some of the electronic properties. For example, a simple but crucially important question is why T_c correlates with the number of CuO_2 -planes in a formula unit. Therefore, theories dealing only with the two-dimensional CuO_2 -planes are insufficient for describing the essential features of the whole HTSC system.

The effect of the multi-layer coupling on Raman scattering spectra has been widely discussed in relation to the polarization dependence of the superconducting gap feature, although the initial discussion was focused on the theory based on a single sheet Fermi surface (FS). The electronic Raman efficiency in the superconducting state was derived by Klein and Dierker [6]. For a single sheet Fermi surface (FS), in the $q \rightarrow 0$ limit the efficiency S is given by

$$S \propto \left[1 - e^{-\hbar\omega/k_B T}\right] \text{Im} \left[\langle \mathbf{g}(\mathbf{k})^2 \mathbf{I}(\mathbf{k}) \rangle_F - \frac{\langle \mathbf{g}(\mathbf{k}) \mathbf{I}(\mathbf{k}) \rangle_F^2}{\langle \mathbf{I}(\mathbf{k}) \rangle_F} \right], \quad (1)$$

where $\langle \rangle_F$ denotes an average over the FS and $\lambda(\mathbf{k})$ is the complex tsuneto function. For a nearly cylindrical FS the imaginary part of $\lambda(\mathbf{k})$ at T=0 has a form

$$\text{Im}[\mathbf{I}(\mathbf{k})] = \frac{4|\Delta(\mathbf{k})|^2}{\sqrt{w^2 - 4|\Delta(\mathbf{k})|^2}}. \quad (2)$$

The Raman vertex γ is described as

$$\mathbf{g}(\mathbf{k}) = \mathbf{e}^L \cdot \mathbf{e}^S + \frac{1}{m} \sum_b \left[\frac{\langle \mathbf{k} | \mathbf{p} \cdot \mathbf{e}^S | b, \mathbf{k} \rangle \langle b, \mathbf{k} | \mathbf{p} \cdot \mathbf{e}^L | \mathbf{k} \rangle}{\epsilon(\mathbf{k}) - \epsilon_b(\mathbf{k}) + \hbar\omega_L} + \frac{\langle \mathbf{k} | \mathbf{p} \cdot \mathbf{e}^L | b, \mathbf{k} \rangle \langle b, \mathbf{k} | \mathbf{p} \cdot \mathbf{e}^S | \mathbf{k} \rangle}{\epsilon(\mathbf{k}) - \epsilon_b(\mathbf{k}) - \hbar\omega_S} \right], \quad (3)$$

where \mathbf{e}^L and \mathbf{e}^S denote the polarization vectors of the incident and scattering light, respectively.

When the incident photon energy $\hbar\omega_L$ is much smaller than the energy difference $\epsilon(\mathbf{k}) - \epsilon_b(\mathbf{k})$ between the initial state $|\mathbf{k}\rangle$ and intermediate state $|b, \mathbf{k}\rangle$, the Raman vertex is reduced to an inverse effective mass tensor $\mu^{-1}(\mathbf{k})$ of the relevant band $\epsilon(\mathbf{k})$,

$$\mathbf{g}(\mathbf{k}) = \mathbf{m}^{-1}(\mathbf{k}) = \frac{m}{\hbar^2} \sum_{\mathbf{a}, \mathbf{b}} e_{\mathbf{a}}^L \frac{\mathcal{I}_{\mathbf{a}}^2 \mathbf{e}_{\mathbf{k}}}{\mathcal{I}_{\mathbf{a}} k_{\mathbf{a}} \mathcal{I}_{\mathbf{b}} k_{\mathbf{b}}} e_{\mathbf{b}}^S, \quad (4)$$

where we take $\alpha, \beta = x, y$ for two-dimensional system.

The second term in Eq.(1) gives rise to a correction of the long range Coulomb effect, so-called screening effect. For structures with D_{4h} symmetry, there are three Raman active channels regarding to the basic ab -plane with A_{1g} , B_{1g} and B_{2g} symmetries. The screening term $\langle \gamma \lambda \rangle_F$ vanishes for the B_{1g} and B_{2g} components but not for A_{1g} . This symmetry dependence of the screening effect on the Raman was experimentally observed in many HTSC. For example, in $\text{Bi}_2\text{Si}_2\text{CaCu}_2\text{O}_{8+\delta}$ (Bi-2212), peaks were found at about 520cm^{-1} in the B_{1g} , 470cm^{-1} in the B_{2g} , and 370cm^{-1} in the A_{1g} spectra, that is, the peak energy $\Delta(B_{1g}) > \Delta(B_{2g}) > \Delta(A_{1g})$ [7]. The symmetry dependence of the peak energy as well as the spectral profile is well explained in terms of a d-wave gap $\Delta(k) = \Delta_0 \cos 2\phi$ [7,8], for which the maximum in the pair-breaking peak

is predicted to appear sharply at $\omega=2\Delta_0$ for the B_{1g} channel, while a rather broad peak is located at a lower frequency $\omega=1.3\Delta_0$ for the B_{2g} channel, reflecting the states near the gap node. The screening effect significantly smears the A_{1g} peak and leads to the low frequency shift of the peak.

Krantz and Cardona have pointed out that this screening effect scenario is valid only in single CuO_2 -layer HTSC, or in the case of completely degenerated bands for the layers [9]. If the bands are non-degenerated, the A_{1g} channel includes the interband Raman process, in addition to the intraband one. The interband scattering, which originates from a mass difference $\mu_i(\mathbf{k})^{-1}-\mu_j(\mathbf{k})^{-1}$ in different sheets of the FS [10], should lead to intense unscreened A_{1g} scattering with a peak $\omega=2\Delta_0$, as in the B_{1g} -channel: $\Delta(B_{1g}) = \Delta(A_{1g})$.

Devereaux and co-workers have theoretically examined this problem in detail for a bilayer system [11, 12] and revealed that the screening effect is still important and smears an intense A_{1g} peak at $\omega=2\Delta_0$, when the interlayer coupling is not very strong. Simultaneously, it has been recognized that the line shape of the A_{1g} scattering is sensitive either to the interlayer coupling or to the FS structure. However, double layer HTSC such as $\text{YBa}_2\text{Cu}_3\text{O}_{7.8}$ (Y-123) and Bi-2212 exhibit nearly the same A_{1g} spectrum. For this problem, there have been many proposals [8,9, 11-17] including the complicated gap function [16] different from a simple d-wave and a correction by spin fluctuation [17]. But, it is still a puzzle why there is no clear effect of interlayer coupling in bilayer HTSC [18, 19]. In other words, accounting for the A_{1g} Raman scattering features is crucial to understand the multi-layer effect on HTSC.

In this context, it is of great interest to investigate the A_{1g} Raman scattering under resonant condition, because the interband Raman process is expected to be enhanced through the resonant part of the Raman vertex between different sheets of FS;

$$\mathbf{g}_{ij}(\mathbf{k}) \approx \frac{1}{m} \frac{\langle i, \mathbf{k} | \mathbf{p} \cdot \mathbf{e} | b, \mathbf{k} \rangle \langle b, \mathbf{k} | \mathbf{p} \cdot \mathbf{e} | j, \mathbf{k} \rangle}{[\mathbf{e}_b(\mathbf{k}) - \mathbf{e}_j(\mathbf{k})]^2 - (\hbar \omega_L)^2}, \quad (5)$$

where $\omega_L \approx \omega_S$ and $\mathbf{e}^L = \mathbf{e}^S \equiv \mathbf{e}$. The electronic Raman scattering has been intensively studied over a wide range of excitation energies in HTSC [20-25]. The resonant phenomena occur at around 2.0 eV and above 2.5 eV. To the best of our knowledge, however, no attempt has been devoted to investigate the A_{1g} problem mentioned above. Recently, the superconductivity-induced changes of the phonon resonance have been found in a bilayer HTSC, suggesting that superconducting order parameter affects the optical transition at 2.1 eV [26].

In this paper, we report resonant Raman scattering of multi-layer HTSC. A strong resonant enhancement of the electronic Raman scattering appears near 2 eV and develops below T_c only in HTSC with three or four CuO_2 layers. A strong A_{1g} peak is observed at an energy $2\Delta(A_{1g})$ close to $2\Delta(B_{1g})$, which suggests unscreened scattering under the resonance condition. This is an indication of interband Raman scattering that is allowed for non-degenerated bands corresponding to the inner and outer CuO_2 -layers. The contribution of the Ca-O vibration phonons to the interlayer coupling is also revealed.

II. EXPERIMENT

In contrast to the intensive studies on Y-123 and Bi-2212, there have been only a few works on three or four layer HTSC, probably because of a lack of high quality single crystals. To extend the research of these materials, we prepared various samples of HTSC with multiple CuO_2 -planes.

Single crystals of Bi-2212 with $T_c=85\text{K}$ and $\text{Bi}_2\text{Si}_2\text{Ca}_2\text{Cu}_3\text{O}_{10+\delta}$ (Bi-2223) with $T_c = 109\text{K}$ were grown by a KCl flux technique [27]. A new crystal growth method for Bi-2223 was developed by optimizing the crucible material, phase and chemical composition of the precursor powder, heat treatment procedure, and evaporation rate of KCl. As a result, we obtained high quality Pb-free Bi-2223 single crystals with a size of $500 \times 500 \times 2 \mu\text{m}^3$. The

details of crystal growth are published elsewhere [28]. The Bi-2212 single crystal is in the slightly overdoped regime, while the doping level of the Bi-2223 crystal is close to the optimum.

A single-phase polycrystalline sample of $\text{Tl}_{0.5}\text{Pb}_{0.5}\text{Sr}_2\text{Ca}_2\text{Cu}_3\text{O}_{9+\delta}$ (Tl-1223) with $T_c=118$ K, the third member ($n=3$) of $\text{TlSr}_2\text{Ca}_{n-1}\text{Cu}_n\text{O}_{2n+3+\delta}$ homologous series [29], was prepared by “space-filling” modification of the encapsulation technique developed previously for the synthesis of Hg-based superconducting cuprates [30]. As-grown samples used for Raman measurements are in the overdoped regime. Polycrystalline samples of $\text{HgBa}_2\text{Ca}_2\text{Cu}_3\text{O}_{8+\delta}$ (Hg-1223), $\text{Hg}(\text{Sr},\text{Ba})_2\text{Ca}_3\text{Cu}_4\text{O}_{10+\delta}$ (Hg-1234) phases - the third ($n=3$) and fourth ($n=4$) members of Hg-based homologous series with general formula $\text{Hg}(\text{Ba}, \text{Sr})_2\text{Ca}_{n-1}\text{Cu}_n\text{O}_{2n+2+\delta}$ [31], were obtained by a high-pressure technique ($t=1000^\circ\text{C}$, $P=5\text{GPa}$). Highly homogeneous oxide precursor powders were prepared by spray-drying and thermal decomposition of the nitrate solutions, from which we obtained Hg-1223 ($T_c=133$ K) and Hg-1234 ($T_c=115$ K) polycrystals with purity higher than 90%. The carrier doping level of the former sample is nearly optimal, while the latter is a little underdoped. In all these multi-layer HTSC, it is generally difficult to change the doping range widely.

The Raman spectra were measured in the pseudo-back scattering configuration with a T64000 Jobin-Yvon spectrometer. The typical spectral resolution was 3cm^{-1} . For excitation several Ar^+ - Kr^+ laser lines ranging from 1.9eV to 2.7eV were used. The power density was about 5 W/cm^2 on the sample surface, and the overheating was estimated to be less than 10K. All the measured spectra were corrected for the spectrometer sensitivity by comparison with that of BaF_2 and the contribution of the Bose factor has been removed. Hereafter we refer to a tetragonal D_{4h} point group with X and Y taken parallel to the Cu-O bonds. In contrast to $B_{1g}(\text{XY})$ and $B_{2g}(\text{X'Y'})$ Raman spectra, the A_{1g} component cannot be exclusively measured by in-plane scattering geometries and was estimated as $I(A_{1g}) = I(\text{XX}) - I(\text{X'Y'})$.

III. RESULTS AND DISCUSSION

Figures 1a and 1c illustrate the A_{1g} -Raman scattering for Bi2212 and Bi2223, respectively, using a blue laser line with an excitation energy $E_{\text{exc}}=2.54\text{eV}$. The frequencies for the three major phonons in the spectrum of Bi2223 are almost the same as those of Bi2212. This is reasonable because the crystal structures of these two compounds are nearly identical except for the number of CuO_2 -planes. The electronic Raman scattering of Bi2223 is also similar to that of Bi2212. The low frequency part of the continuum exhibits a clear redistribution below T_c , owing to the formation of a superconducting gap. The gap peak is very broad and centered at 450 cm^{-1} that is slightly larger than 390 cm^{-1} for Bi2212, probably because of the higher T_c of Bi2223.

At the orange excitation ($E_{\text{exc}}=2.18\text{eV}$), there appears a remarkable difference in the superconducting response between the two spectra. As shown in Figs.1b and 1d, in contrast to the almost unchanged spectrum of Bi2212, the 2Δ -peak in the Bi2223 spectrum is enhanced and located at a higher frequency than that for the blue excitation. Furthermore, very strong additional phonon lines are observed at 260 cm^{-1} and 390 cm^{-1} .

In Fig.2a, the spectra at four different temperatures demonstrate a gradual development of the spectrum below T_c peaking at 580 cm^{-1} . Figure 2b illustrates the temperature dependence of the Raman intensity at 580 cm^{-1} that is normalized at 1000 cm^{-1} . It is clearly seen that a dramatic increase in the peak intensity as well as its resonance behavior sets in just below T_c .

Figure 3a displays the A_{1g} spectra of Bi2223 at 10K for several excitation energies. The electronic intensity between 200 to 900 cm^{-1} rapidly grows with decreasing E_{exc} , and consequently shows a strong 2Δ -peak at 580 cm^{-1} . Simultaneously, the weak phonon bumps in

the blue spectrum become stronger and nearly symmetric lines at 260 cm^{-1} and 390 cm^{-1} . The manifestation of these phonons is closely related to the growth of the 580 cm^{-1} gap peak.

Comparing the A_{1g} -spectrum with the B_{1g} - and B_{2g} -spectra at 10K for $E_{\text{exc}}=2.18\text{eV}$ (Fig.3b), we immediately find that the A_{1g} -peak position coincides with that for B_{1g} . Therefore, “in resonance”, the relative positions of the pair breaking peaks in the A_{1g} , B_{1g} , and B_{2g} channels is $2\Delta(A_{1g}) = 2\Delta(B_{1g}) > 2\Delta(B_{2g})$, as predicted theoretically for a d-wave multi-layer superconductor [9, 11, 12] but not observed to date. This implies that the resonant part of the A_{1g} scattering is primarily free from screening effect due to the long range Coulomb force [12] and/or collective spin fluctuation [17]. Note that the profile and the peak position do not change with changing E_{exc} , in the B_{1g} - and B_{2g} -spectra (not shown here). The appearance of a high frequency bump at around $\omega=3\Delta_0$ in the B_{1g} -polarization might originate from electronic excitations around the van Hove singularity [12, 32].

Figure 4a shows the resonance behavior of the height of the $2\Delta(A_{1g})$ -peak at 580cm^{-1} in Bi-2223, in comparison with the almost E_{exc} -independent behavior of the $2\Delta(A_{1g})$ -peak at 390cm^{-1} in Bi-2212. Here, the 2Δ -peak intensities are normalized by the continuum intensity at 1000cm^{-1} . In Fig.4b, the renormalized phonon intensities $I_p = A\Gamma q^2$ [33, 34] for the 260 and 390 cm^{-1} phonon lines in Bi-2223 are plotted as a function of E_{exc} . For Bi-2223, the resonant phenomenon is evident, although the data does not reach a maximum. The relevant energy level is presumably located at about 2eV or below. In contrast, the relative intensity of the $2\Delta(A_{1g})$ -peak in Bi-2212 is almost independent of the excitation energy, as was observed in Tl-2201 [22].

The Raman vertex γ has a resonance character if the photon energy $\hbar\omega_L (=E_{\text{exc}})$ is close to the electronic excitation energy $\epsilon_b - \epsilon_j$, as is seen in eq.(5). This strongly enhances the Raman scattering efficiency S in Eq.(1) [10]. In Fig.4, the phonon intensity exhibits a similar E_{exc} -dependence. Therefore, it is supposed that the phononic Raman scattering is resonant to

the same energy level.

The enhanced phonon lines at 260 and 390 cm^{-1} in Bi-2223 can be ascribed to the A_{1g} -vibration of Ca with oxygen in the outer CuO_2 -planes, following the mode assignment of the phonon lines in Hg-1234 [34]. The asymmetric line shapes of these phonons result from quantum interference to the electronic counter part. Thus, it is expected that the bare phonon frequency Ω_0 and line-width Γ_0 are renormalized by the electronic response $\chi(\omega)=R+i\rho$ through the electron-phonon coupling V ; $\Omega=\Omega_0+V^2R$ and $\Gamma=\Gamma_0+V^2\rho$, and that the frequency and line-width anomalies below T_c are induced by the A_{1g} electronic response peaking at 580 cm^{-1} . To estimate this phonon self-energy effect correctly, one have to analyze the Raman spectrum using the Green's function approach [35-38] or sophisticated Fano approach [39, 40]. In both approaches one introduces an analytical function to describe the background electronic response ρ . In the present case, however, the background consists of two components with different resonance behaviors. One exhibits a broad spectrum peaking at about 300 cm^{-1} and the other, which mainly interacts with the relevant phonons, shows a sharp pair-breaking peak at 580 cm^{-1} . For the time being, we use a "standard" Fano approach [33, 34, 37]. As was shown in our previous paper [37], for a single component background the "standard" Fano procedure and the Green's function analysis give essentially the same renormalized phonon parameters (frequency, line-width and intensity) both above and below T_c , if we assume an appropriate electronic background function $g(\omega)$ in the Fano analysis. In the following analysis $g(\omega)$ is assumed to have a steep slope, reflecting a pair-breaking peak near this phonon.

Figure 5 shows the temperature dependence of the phonon parameters for the 390 cm^{-1} phonon mode at $E_{\text{exc}}=2.18\text{eV}$. Remarkable softening and broadening occur below T_c , owing to development of the $2\Delta(A_{1g})$ -peak at 580 cm^{-1} . The large amount of softening (30 cm^{-1} ; 8% of the frequency) demonstrates the strong interaction with the electronic system. Similar strong softening and broadening were also observed in Hg-1234 by Hadjiev *et al.* [34]. It may be

worth to note that the largest softening of the Ag-phonon in double layer Y-123 is only 3% [41], while it is negligibly small in mono-layer Hg-1201 [42]. The asymmetry parameter q is described as $q=[V(T_p/T_e)+V^2R]/\Gamma$, where T_p and T_e are the phononic and electronic Raman matrix elements. The small $|q|$ above T_c and the large $|q|$ below T_c in Fig.5 illustrate the asymmetric line shape above T_c and nearly symmetric below T_c , respectively. Since the second term contribution is estimated from Ω and Γ as $[(V^2R)_{110K}-(V^2R)_{10K}]/\Gamma \approx 1.3$, the large change in $|q|$ below T_c predominantly originates from the first term.

In Fig. 6, we present the 10K-Raman scattering from the samples of polycrystalline Hg-1234, Hg-1223, Tl-1223 and the single crystal of Y-123 at red (1.92eV) and blue (2.54 eV) laser excitations. For Hg-1234, the strong enhancement of the Ca-phonon peaks, accompanied by the strong $2\Delta(A_{1g})$ -peak at 600 cm^{-1} , was first observed at $E_{exc}=1.92\text{eV}$ by Hadjiev *et al.* [34]. We found that this enhancement is suppressed when E_{exc} increases, namely, that this is a resonance phenomenon. From Fig.6, it is concluded that resonance behavior of the 2Δ -peak and the Ca-phonons is commonly observed in HTSC with three or four CuO_2 -layers in a formula unit, but not in the compounds with a double CuO_2 -layer such as Y-123 or Bi-2212. Therefore, the superconductivity-induced resonance is closely related to the presence of the inner CuO_2 -layer sandwiched by the outer CuO_2 -layers. Moreover, since this phenomenon is observed not only in the optimal doping level (Bi-2223 and Hg-1223) but also in the underdoped Hg-1234 and the overdoped Tl-1223, it turns out that the phenomenon is little sensitive to the average doping level for the multiple layers.

The importance of the inner CuO_2 -layer and the Ca-phonons in the present resonance phenomenon tells us that the interband Raman scattering plays a major role. The Ca-atoms are located just between the inner- and outer- CuO_2 layers and thus A_g Ca-phonons possibly mediate the interband electronic excitations. If the bands originating from the two CuO_2 -layers were degenerate, the interband part should vanish. Therefore, the present results indicate that

the energy bands for the inner and the outer CuO_2 -layers are slightly different. In this Raman process an electron-like (or hole-like) quasiparticle is created above the gap Δ_{inner} of the inner CuO_2 -layer, whereas a hole-like (or electron-like) quasiparticle is above the gap Δ_{outer} of the outer CuO_2 -layer. From our results it can be deduced that the gap energy Δ_{inner} for the inner-layer is almost the same as Δ_{outer} for the outer-layers.

At the blue excitation the interband Raman scattering is very weak, compared to the intraband channels. It is activated by the resonance. A plausible candidate for the resonance is the one with the optical transition to the upper Hubbard band ($\sim 2\text{eV}$), the oscillator strength of which may survive owing to the underdoped nature of the inner CuO_2 -plane [43, 44]. Recently, it has been reported from the nuclear magnetic resonance experiments that the doping level of the inner layer is lower than the outer layer in Cu- and Hg-based three (or four)-layer HTSC [5]. The reason why the resonance of the interband Raman process appears only below T_c is currently unclear. The incoherent c -axis conduction in the normal state turns to a coherent transport below T_c owing to a Josephson coupling between the CuO_2 -layers, which may help the interlayer Raman process. As a possible change in the resonance condition, a superconductivity-induced change in dielectric function in the visible light region has been reported on Bi-2212 by some optical measurements [45]. This might be related to the present observation of diminishing a resonance behavior below T_c .

IV. CONCLUSIONS

In conclusion, we observed resonant Raman scattering below T_c in the A_{1g} -spectra of three or four CuO_2 -layer HTSC. For Bi-2223, the A_{1g} pair-breaking peak shifts from 450cm^{-1} ($\approx 6k_B T_c$) to 580cm^{-1} ($\approx 8k_B T_c$), when the excitation energy changes from 2.54eV to 2.18eV . As a result, in resonance, the relative positions of the pair breaking peaks are $2\Delta(A_{1g}) =$

$2\Delta(B_{1g}) > 2\Delta(B_{2g})$, as was theoretically predicted for d -wave multi-layer superconductors but not observed previously. In addition to the changes in the $2\Delta(A_{1g})$ peak position, the intensities of the $2\Delta(A_{1g})$ peak and the Ca-phonons show a remarkable enhancement. We attribute these pronounced spectral changes to the appearance of an interband Raman scattering process that is mediated by the Ca-phonons, resulting from a coupling of the slightly different energy bands for the inner- and outer-CuO₂-layers. The resonance at around 2eV excitation energy enhances the unscreened Raman scattering due to multi-sheet effects. This result emphasises recalls us to the importance of resonant Raman studies from both the experimental and theoretical viewpoints.

ACKNOWLEDGMENTS

The authors thank Y. Fudamoto and Yu. Eltsev for experimental assistance and J. Quilty for helpful discussions. This work was supported by the New Energy and Industrial Technology Development Organization (NEDO) as Collaborative Research and Development of Fundamental Technologies for Superconductivity Applications.

* Permanent address: A.F.Ioffe Physical-Technical Institute, 194021 St.Petersburg, Russia.

- [1] As a review, S. L. Cooper and K. E. Gray, *Physical Properties of high Temperature Superconductors IV*, ed. by D. M. Ginsberg (Work Scientific), pp.61-188 (1994).
- [2] M. Tachiki, T. Koyama, and S. Takahashi, *Phys. Rev. B* **50**, 7065 (1994); Y.Matsuda *et al.*, *Phys. Rev. Lett.* **75**, 4512 (1995).
- [3] D. Van der Marel and A. Tsvetkov, *Czech. J. Phys.* **46**, 3165 (1996); V. Zelezny *et al.*, *Phys. Rev. B* **63**, 060502(R) (2001).
- [4] D.L.Feng *et al.*, *Phys. Rev. Lett.* **88**, 107001 (2001).
- [5] Y. Tokunaga *et al.*, *Phys. Rev. B* **61**, 9707 (2000); H. Kotegawa *et al.*, *Phys. Rev. B* **64**, 064515 (2001).
- [6] M. V. Klein, S. B. Dierker, *Phys. Rev. B* **29**, 4976 (1984).
- [7] T. P. Devereaux *et al.*, *Phys. Rev. Lett.* **72**, 396 (1994); T. P. Devereaux *et al.*, *Phys. Rev. Lett.* **72**, 3291 (1994).
- [8] T. P. Devereaux and D. Einzel, *Phys. Rev. B* **51**, 16336 (1995); *ibid* **54**, 15548 (1996).
- [9] M. Krantz and M. Cardona, *Phys. Rev. Lett.* **72**, 3290 (1994); *J. of Low Temp Phys* **99**, 205 (1995).
- [10] M.Cardona, in *Light Scattering in Solids II*, M.Cardona, G.Güntherodt, Eds. (Springer-Verlag, Berlin, 1982), pp.19-178.
- [11] T. P. Devereaux, D. Einzel, *Phys. Rev. B* **51**, 16336 (1995); T. P. Devereaux, *SPIE* **2696**, 230 (1996).
- [12] T.P.Devereaux, A. Virosztek, and A. Zawadowski *Phys. Rev. B* **54**, 12523 (1996).
- [13] D. Branch, J. P. Carbotte, *Phys. Rev. B* **54**, 13288 (1996).
- [14] F. Wenger and M. Käll, *Phys. Rev. B* **55**, 97 (1997).
- [15] D. Manske, C. T. Rieck, R. Das Sharma, A. Bock, and D. Fay, *Phys. Rev. B* **56**, R2940 (1997); **58**, 8841 (1998).

- [16] T. Strohm and M. Cardona, Phys. Rev. B **55**, 12725 (1997); **58**, 8839 (1998).
- [17] F. Venturini, U. Michelucci, T. P. Devereaux, and A. P. Kampf, Phys. Rev. B **62**, 15204 (2000).
- [18] M. Cardona, Physica C **317-318**, 30 (1999);
- [19] D. Branch, J. P. Carbotte, J. of Superconductivity **13**, 535 (2000).
- [20] E. T. Heyen *et al.*, Phys. Rev. Lett. **65**, 3048 (1990).
- [21] D. E. Wake *et al.*, Phys. Rev. Lett. **67**, 3728 (1991).
- [22] M. Kang, G. Blumberg, M. V. Klein, N. N. Kolesnikov, Phys. Rev. Lett. **77**, 4434 (1996).
- [23] G. Blumberg, M. Kang, M. V. Klein, K. Kadowaki, C. Kendziora, Science **278**, 1427 (1997).
- [24] A. G. Panfilov, M. F. Limonov, A. I. Rykov, S. Tajima, A. Yamanaka, Phys. Rev. B **57**, R5634 (1998).
- [25] H. L. Liu, G. Blumberg, M. V. Klein, P. Guptasarma, D. G. Hinks, Phys. Rev. Lett. **82**, 3524 (1999).
- [26] S. Ostertun, J. Kiltz, A. Bock, U. Merk, and T. Wolf, Phys. Rev. B **64**, 064521 (2001).
- [27] L. F. Schneemeyer *et al.*, Nature **332**, 422 (1988).
- [28] S. Lee, A. Yamamoto, and S. Tajima, Physica C **357-360**, 341 (2001).
- [29] M. A. Subramanian, *et al.*, Science **242**, 249 (1988).
- [30] S. Lee, M.-O. Mun, M.-K. Bae, and S.-I. Lee, J. Mater. Chem. **4**, 991 (1994).
- [31] S. N. Putilin, E. V. Antipov, O. Chmaissem, and M. Marezio, Nature **362**, 226 (1993); E. V. Antipov, *et al.*, Physica C **215**, 1 (1993).
- [32] D. Branch and J. P. Carbotte, Phys. Rev. B **52**, 603 (1995).
- [33] C. Thomsen, in *Light Scattering in Solids VI*, M. Cardona, G. Guntherodt, Eds. (Springer-Verlag, Berlin, 1991).
- [34] V. G. Hadjiev *et al.*, Phys. Rev. B **58**, 1043 (1998).

- [35] X. K. Chen, E. Altendorf, J. C. Irwin, R. Liang, and W. N. Hardy, *Phys. Rev. B* **48**, 10530 (1993).
- [36] X. K. Chen, J. C. Irwin, R. Liang, and W. N. Hardy, *Physica C* **227**, 113 (1994).
- [37] M. Limonov, D. Shantsev, S. Tajima, and A. Yamanaka, *Phys. Rev. B* **65**, 024515 (2002).
- [38] J. W. Quilty, S. Tajima, S. Adachi and A. Yamanaka, *Phys. Rev. B* **63**, 100508(R) 2001.
- [39] A. Bock *et al.*, *Phys. Rev. B* **60**, 3532 (1999).
- [40] A. Bock, *Annalen der Physik* **8**, 441 (1999).
- [41] M. F. Limonov, A.I. Rykov, S. Tajima, and A. Yamanaka. *Phys. Rev. B* **61**, 12412 (2000).
- [42] M. C. Krantz, C. Thomsen, Hj. Mattausch, and M. Cardona, *Phys. Rev. B* **50**, 1165 (1994).
- [43] The excitation across the charge transfer gap from O2p to Cu3d upper Hubbard band is commonly observed in the optical spectra of undoped insulator compounds of HTSC. See, for example [42]. When carriers are doped, this excitation is rapidly suppressed, but weakly remains in the underdoped regime.
- [44] Y. Tokura *et al.*, *Phys. Rev. B* **41**, 11657 (1990)
- [45] M. Ruebhausen *et al.*, *Phys. Rev. B* **63**, 224514 (2001); A. F. Santander-Syro *et al.*, cond-mate/0111539; D. van der Marel *et al.*, to be published.

FIGURE CAPTIONS

Fig.1 A_{1g} Raman spectra of Bi2212 for $E_{exc}=2.54\text{eV}$ (a) and for $E_{exc}=2.18\text{eV}$ (b). A_{1g} Raman spectra of Bi2223 for $E_{exc}=2.54\text{eV}$ (c) and for $E_{exc}=2.18\text{eV}$ (d). In all cases, the spectra are shown above and below T_c by thin lines and thick lines, respectively. All spectra are corrected for the Bose-Einstein statistical factor.

Fig.2 (a) Temperature dependence of the Raman spectra of Bi2223 for $E_{exc}=2.18\text{eV}$. All spectra are corrected for the Bose-Einstein statistical factor. (b) Temperature dependence of the height of the $2\Delta(A_{1g})$ -peak at 580cm^{-1} ($I_{580\text{cm}^{-1}} / I_{1000\text{cm}^{-1}}$) in Bi-2223 spectra for $E_{exc}=2.54\text{eV}$ and for $E_{exc}=2.18\text{eV}$.

Fig.3 (Color) (a) A_{1g} Raman spectra of Bi2223 at $T=10\text{K}$ with various excitation lines. Here the continuum intensity at 1000cm^{-1} is assumed to be unity. (b) A_{1g} , B_{1g} , and B_{2g} spectra with $E_{exc}=2.18\text{eV}$ at $T=10\text{K}$.

Fig.4 (a) The height of the $2\Delta(A_{1g})$ -peak at 580cm^{-1} ($I_{580\text{cm}^{-1}} / I_{1000\text{cm}^{-1}}$) in Bi-2223 spectra, compared with the height of the $2\Delta(A_{1g})$ peak at 390cm^{-1} ($I_{390\text{cm}^{-1}} / I_{1000\text{cm}^{-1}}$) in Bi-2212 spectra. (b) The resonance Raman profiles of the renormalized phonon intensities I_p for the 260 and 390cm^{-1} phonon lines in Bi-2223 spectra. $T=10\text{K}$. The lines are guides to the eye.

Fig.5 Temperature dependencies of the phonon parameters of the 390cm^{-1} phonon for the Bi-2223 single crystals at $E_{exc}=2.18\text{eV}$: (a) renormalized frequency Ω , (b) renormalized linewidth \mathcal{T} , (c) the Fano parameter $-q$. The solid lines display the expected T-dependencies for the uncoupled frequency and linewidth [37].

Fig.6 The 10K -Raman spectra of the polycrystalline Hg-1234 (a), Hg-1223 (b), Tl-1223 (c), and the Y-123 single crystal (d) obtained at $E_{exc}=1.92\text{eV}$ (solid curves) and 2.54eV (dashed curves). In (d) panel, the spectrum has A_{1g} symmetry, while the spectra in (a, b, c) panels are polarized ones. Intensities of the data for 2.54eV in (d) are multiplied by 3.

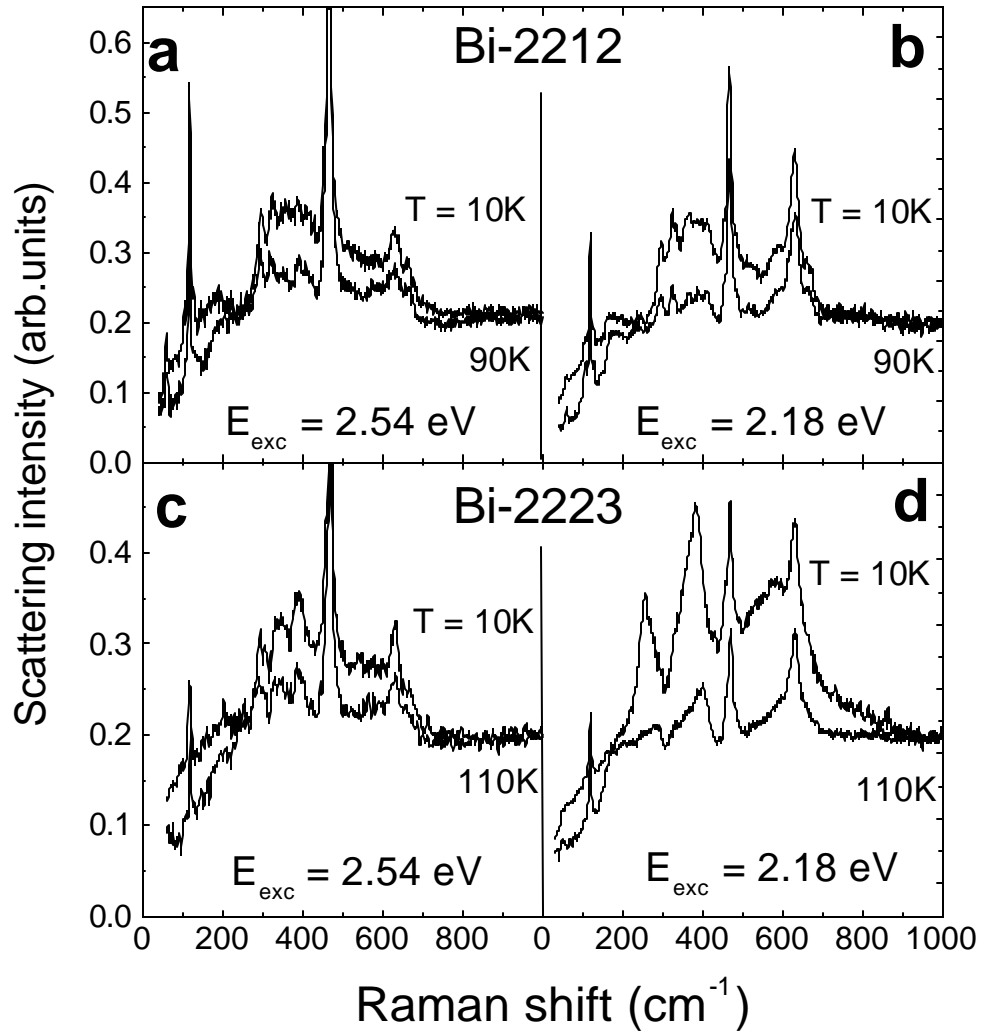


Fig.1 Limonov e.a.

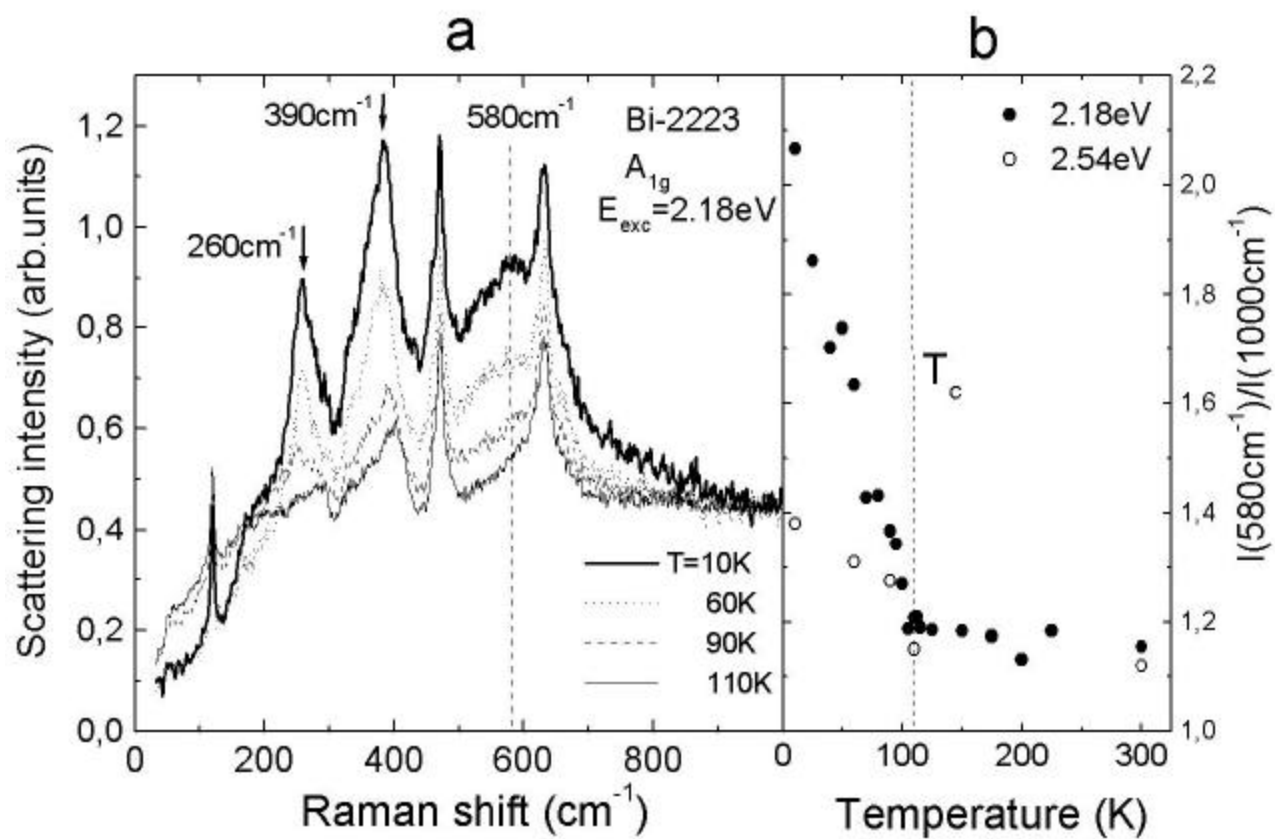


Fig.2 Limonov e.a.

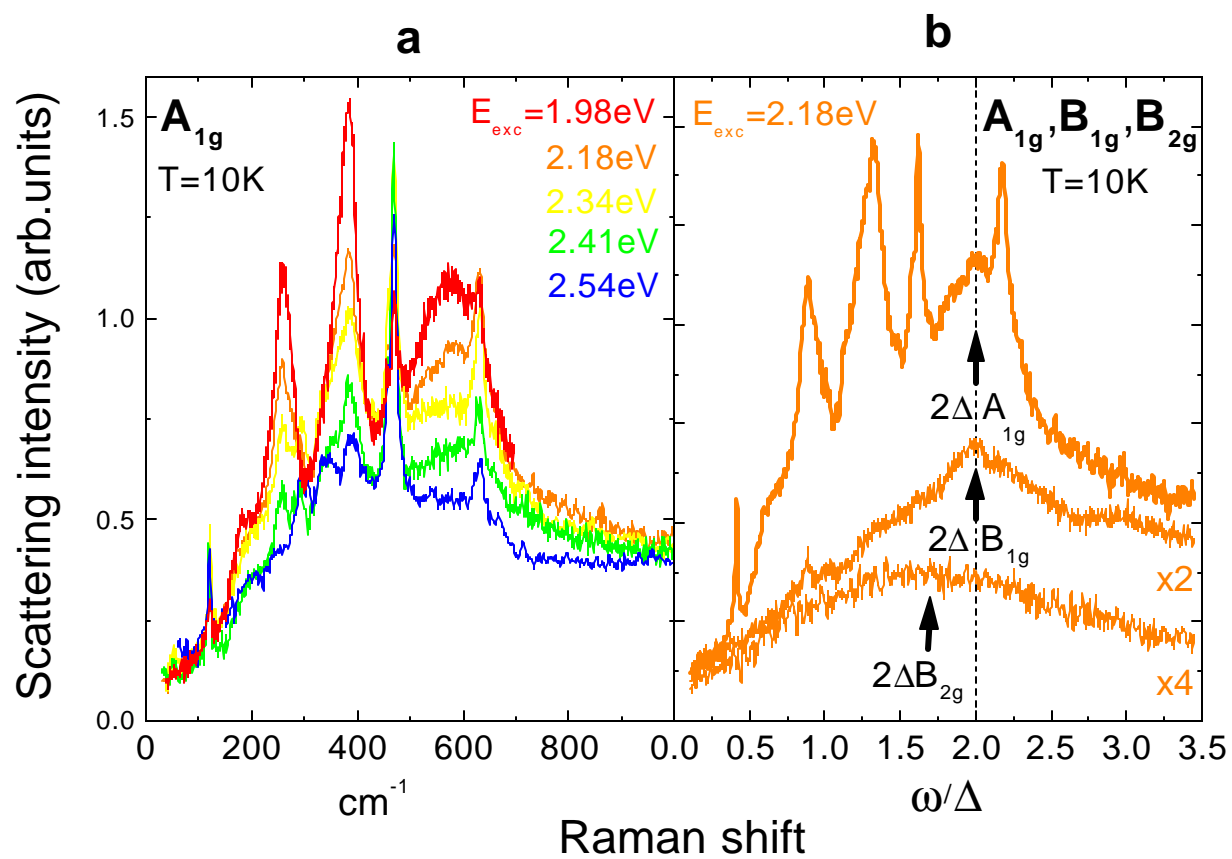


Fig.3 Limonov e.a.

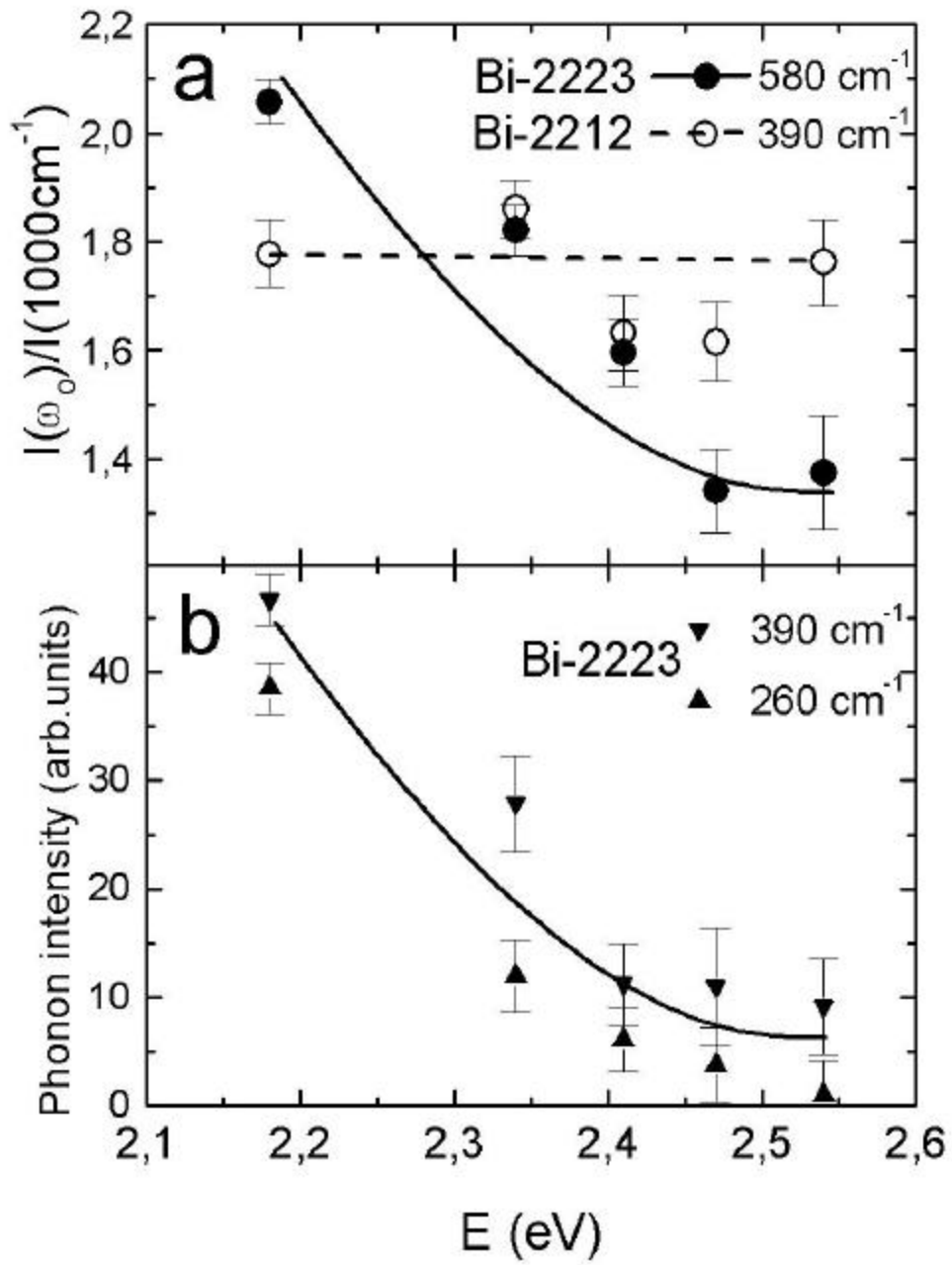


Fig.4 Limonov e.a.

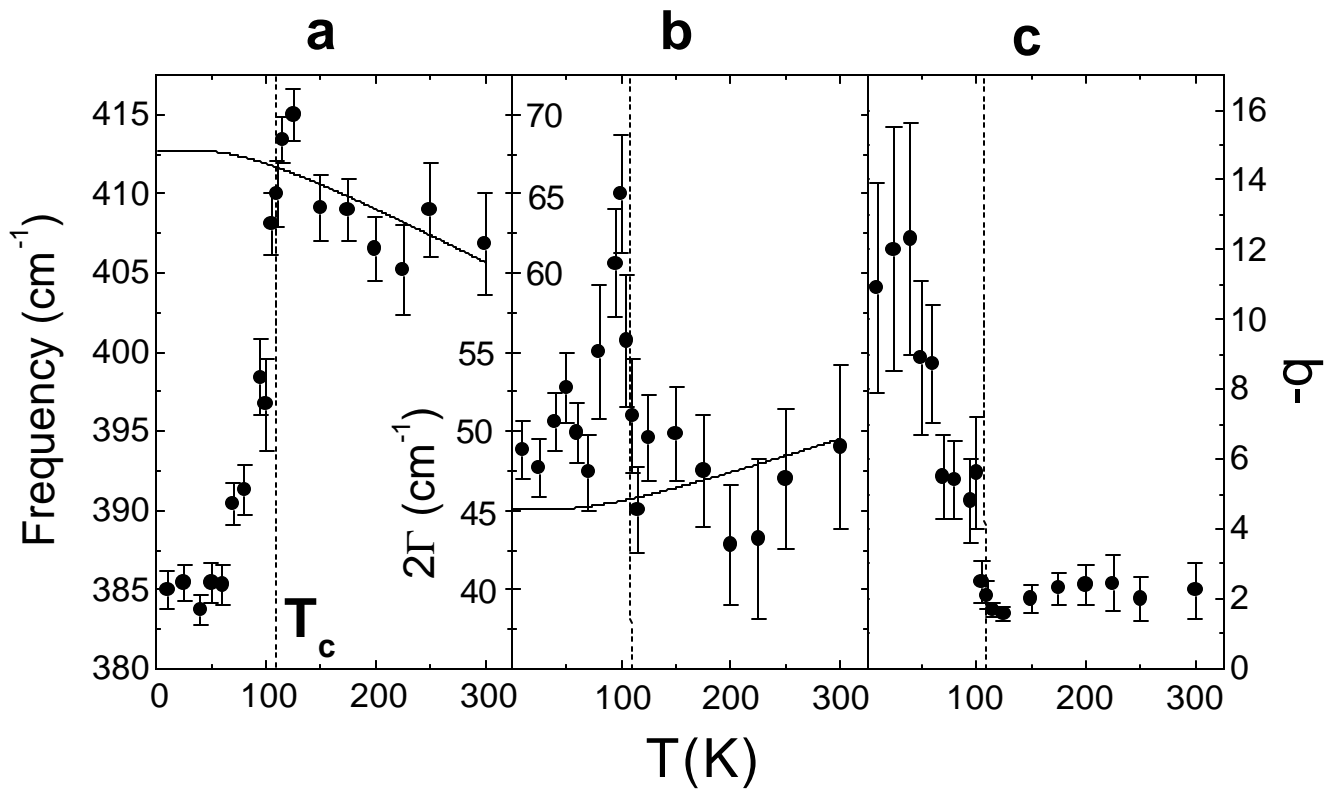


Fig.5 Limonov e.a.

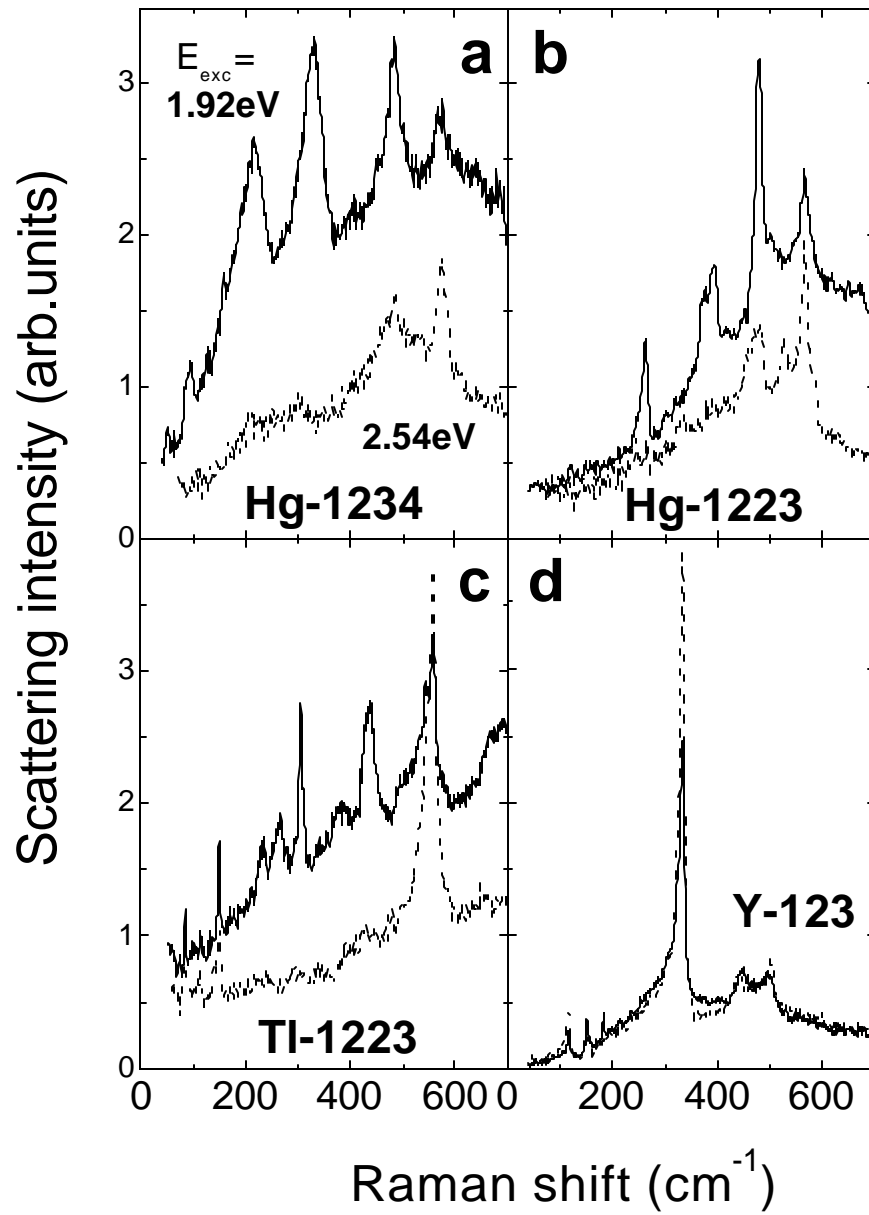


Fig.6 Limonov e.a.